Blood Stasis Imaging Predicts Cerebral Microembolism during Acute Myocardial Infarction

Antonia Delgado-Montero, MD, PhD, Pablo Martinez-Legazpi, MEng, PhD, M. Mar Desco, MD, PhD, Daniel Rodríguez-Pérez, MPhys, PhD, Fernando Díaz-Otero, MD, Lorenzo Rossini, AEng, PhD, Candelas Pérez del Villar, MD, PhD, Elena Rodríguez-González, MD, Christian Chazo, AEng, Yolanda Benito, DCS, DVM, Oscar Flores, AEng, PhD, José Carlos Antoranz, MPhys, PhD, Francisco Fernández-Avilés, MD, PhD, Juan C. del Álamo, AEng, PhD, and Javier Bermejo, MD, PhD, *Madrid, Spain; and San Diego, California*

Background: Cardioembolic stroke is a major source of mortality and disability worldwide. The authors hypothesized that quantitative characterization of intracardiac blood stasis may be useful to determine cardioembolic risk in order to personalize anticoagulation therapy. The aim of this study was to assess the relationship between image-based metrics of blood stasis in the left ventricle and brain microembolism, a surrogate marker of cardiac embolism, in a controlled animal experimental model of acute myocardial infarction (AMI).

Methods: Intraventricular blood stasis maps were derived from conventional color Doppler echocardiography in 10 pigs during anterior AMI induced by sequential ligation of the mid and proximal left anterior descending coronary artery (AMI-1 and AMI-2 phases). From these maps, indices of global and local blood stasis were calculated, such as the average residence time and the size and ratio of contact with the endocardium of blood regions with long residence times. The incidence of brain microemboli (high-intensity transient signals [HITS]) was monitored using carotid Doppler ultrasound.

Results: HITS were detected in 0%, 50%, and 90% of the animals at baseline and during AMI-1 and AMI-2 phases, respectively. The average residence time of blood in the left ventricle increased in parallel. The residence time performed well to predict microemboli (C-index = 0.89, 95% CI, 0.75–1.00) and closely correlated with the number of HITS ($R = 0.87$, $P < .001$). Multivariate and mediation analyses demonstrated that the number of HITS during AMI phases was best explained by stasis. Among conventional echocardiographic variables, only apical wall motion score weakly correlated with the number of HITS ($R = 0.3$, $P = .04$). Mural thrombosis in the left ventricle was ruled out in all animals.

Conclusions: The degree of stasis of blood in the left ventricle caused by AMI is closely related to the incidence of brain microembolism. Therefore, stasis imaging is a promising tool for a patient-specific assessment of cardioembolic risk. (J Am Soc Echocardiogr 2020;33:389-98.)

Keywords: Blood stasis, Stroke, Acute myocardial infarction, Anticoagulation therapy, Doppler echocardiography

From the Department of Cardiology, Hospital General Universitario Gregorio Marañón, Facultad de Medicina, Universidad Complutense de Madrid, Instituto de Investigación Sanitaria Gregorio Marañón, and CIBERCV (A.D.-M., P.M.-L., C.P.V., E.R.-G., C.C., Y.B., F.F.-A., J.B.), the Department of Mathematical Physics and Fluids, Facultad de Ciencias, Universidad Nacional de Educación a Distancia (M.M.D., D.R.-P., J.C.A.), and the Department of Neurology, Hospital General Universitario Gregorio Marañón, Instituto de Investigación Sanitaria Gregorio Marañón (F.D.-O.), Madrid; Department of Bioengineering and Aerospace Engineering, Universidad Carlos III de Madrid, Spain (O.F.); and the Mechanical and Aerospace Engineering Department and Institute for Engineering in Medicine, University of California, San Diego, San Diego, California (L.R., J.C.Á.).

This study was supported by grant PI15/02211, Rio Hortega (CM17/00144), and Juan Rodés fellowships (JR15/00039) from Instituto de Salud Carlos III; grant DPI2016-75706-P and a Juan de la Cierva fellowship (IJCI-2014-19507) from Ministerio de Economía y Competitividad; synergy grant Y2018/BIO-4858-PREFI-CM from Comunidad Autónoma de Madrid; the European Union - European Regional Development Fund; by the Spanish Society of Cardiology (ISBI-DCM); by the University of California,San Diego, CTRI Galvanizing Engineering and Medicine Program; American Heart Association grant 16GRNT27250262; and National Institutes of Health UC CAI grant CII4560. P.M.-L. was also funded by CIBERCV. P.M.-L., L.R., J.C.A., and J.B. are inventors of a method for quantifying intracardiac stasis from imaging data under a Patent Cooperation Treaty patent application (WO2017091746A1).

Reprint requests: Pablo Martinez-Legazpi, MEng, PhD, Department of Cardiology, Hospital General Universitario Gregorio Marañón, Dr. Esquerdo 46, 28007 Madrid, Spain (E-mail: *legazpi.pablo@cibercv.es*).

0894-7317

https://doi.org/10.1016/j.echo.2019.09.020

Abbreviations

2D = Two-dimensional

AMI = Acute myocardial infarction

CDV = Color Doppler velocimetry

HITS = High-intensity transient signals

LAD = Left anterior descending coronary artery

LV = Left ventricular

RT = Residence time

Ischemic stroke is a devastating complication of acute myocardial infarction (AMI). Despite the widespread use of revascularization and antithrombotic therapies, the incidence of ischemic stroke is still approximately 1% during the in-hospital stay of an AMI episode.[1] During the 2 following years, incidence increases to 3% to 5%.[2] Although clinical risk factors for ischemic stroke after AMI have been well identified (age, diabetes mellitus, and renal insufficiency, among others), the predictive value of clinically based scores for guiding individual therapy is still limited.[2]

In the absence of atrial fibrillation, most AMI-related ischemic strokes are believed to result from left ventricular (LV) thrombosis.[3] In fact, mural LV thrombi are identified in 15% to 25% of anterior AMIs, the AMI location most prone to ischemic stroke.[4-6] However, the chance for anticipating stroke by detecting mural thrombosis is low given the limited sensitivity of imaging techniques[6] and the limited chance of the patient being scanned after mural thrombosis develops but before thrombotic material is embolized.[4] Both systemic and local factors favor thrombosis in AMI. A global inflammatory state[7] induces a systemic procoagulation condition, whereas the disrupted endocardial layer favors platelet activation.

The third factor predisposing to intraventricular thrombosis is blood stasis. Global and regional LV chamber abnormalities disturb physiologic blood transit, impairing intraventricular blood washout and triggering the coagulation cascade. This is believed to be the most relevant mechanism responsible for ischemic strokes in the chronic phase after the AMI episode. However, conventional methods for addressing blood washout are subjective and thus have limited clinical value.[8] In recent years, imaging-based methods have been developed to characterize blood transport[9] and even obtain patient-specific maps of intraventricular blood stasis.[10,11] We hypothesized that stasis mapping may be useful to quantify the risk for cardioembolic stroke after AMI, eventually providing physicians with patient-specific metrics of cardioembolic risk.

Subclinical microemboli, detected by transcranial Doppler as high-intensity transient signals (HITS), are related to a number of cardiac procedures[12] and conditions.[13] In the setting of AMI, microemboli have been identified in 17% of patients.[14] Because microemboli correlate with risk for ischemic stroke, silent brain infarct, and neuropsychologic deficits,[15] the number of HITS is a well-validated surrogate outcome in clinical[16] and preclinical trials.[17] On this basis, the present study was designed to assess the value of echocardiography-derived metrics of intraventricular blood stasis to predict the risk for cardioembolism, quantified by the incidence of cerebral microembolisms taking place during an anterior AMI.

METHODS

Experimental Preparation and Protocol

We designed an open-chest repeated-measurements experiment of two sequential anterior AMIs of different sizes to maximize the statistical power while minimizing the number of required animals. We studied 10 adult minipigs (36 ± 3 kg, seven male). Anesthetic induction was made with intravenous propofol (1.5 mg/kg body weight) and fentanyl (5 μg/kg). Animals were endotracheally intubated and ventilated mechanically without end-expiratory positive pressure. We maintained complete anesthesia and relaxation by propofol infusion (0.2 mg/kg/min), atracurium (0.3 mg/kg/h), and repetitive intravenous boluses of fentanyl (0.05 mg). We provided cardiorespiratory support throughout the total duration of the procedure, including inotropic support and defibrillation as needed. We continuously monitored the abolition of eye reflexes, blood pressure, and heart rate to guarantee deep anesthesia. We ensured optimal oxygenation and ventilation by repeated arterial blood gas analyses. To prevent confusion, we avoided using any antithrombotic therapies (heparin, antiplatelet of fibrinolytic agents), and we did not perform any left-heart or arterial catheterization procedures.

After median sternotomy, we surgically exposed the left common carotid artery to fit the transcranial Doppler probe directly on its adventitia. Then, after opening the pericardium, we ligated the left anterior descending coronary artery (LAD) in the middle (mid LAD) and proximal (proximal LAD) segments sequentially to induce two AMI sizes in each animal. We performed a sequential echocardiography and vascular (continuous carotid examination for 30 min) Doppler data acquisition protocol at baseline and during two phases of experimental anterior AMI in each animal (see below and Figure 1). The AMI phases were separated by 90 min for hemodynamic stabilization. At the end of the experiment, animals were euthanized using intravenous sodium pentobarbital (100 mg/kg). The local institutional animal care committee approved the experimental protocol. All animal procedures were in accordance with guidelines from European Union Directive 2010/63/EU.

Carotid Doppler: HITS Measurement and Analysis

We used carotid Doppler ultrasound to measure HITS by placing an 8-MHz transducer (MultiDop T, DWL, QL software version 2.1; Compumedics, Dresden, Germany) covered with ultrasound gel on the exposed left carotid artery. We secured the probe to the animal's neck in a fixed position with an insonation angle of 20° and scanned continuously during 30 min in each phase. We analyzed HITS using the proprietary software of the Doppler system. We set the two insonation depths of the bigate probe at 4 to 6 mm and 8 to 10 mm, the sample volume to 3 to 4 mm^3, the velocity scale to 100 cm/sec, power to 60 ± 10 mW/cm^2, and the high-pass filter to 120 Hz.[18] HITS were automatically identified and differentiated from artifacts, and their time of occurrence and signal intensity (in decibels) were registered (Figure 1). Detection of cerebral HITS was based on recommended criteria and refined using a detection threshold of 15 dB above the background level to avoid false positives at baseline.[18]

Image Acquisition and Analysis

We performed epicardial echocardiographic examinations using a Vivid 7 scanner and phased-array 2- to 4-MHz transducers (GE Healthcare, Little Chalfont, United Kingdom). We obtained two-dimensional (2D) sequences from epicardial apical views to ensure complete apical visualization using a gel pad when necessary, avoiding foreshortening. Also, we obtained high-quality epicardial B-mode four-, two-, and three-chamber sequences with a near-field focus, optimized for comprehensive visualization of the LV apex. LV volumes and ejection fraction were calculated from these views using the modified

HIGHLIGHTS

- Blood stasis mapping can be quantified using conventional color-Doppler echocardiography.
- Stasis indices perform well to predict the microemboli generated during an anterior AMI.
- Stasis imaging is a promising tool for patient-specific assessment of cardioembolic risk.

biplane Simpson's rule in EchoPAC version 110.1.2 (GE Healthcare). We used pulsed-wave Doppler spectrograms of LV transmitral and ejection flow to characterize filling waves and to determine the timing of the cardiac events and used these data for stasis mapping calculations (see below). Two level III experts in cardiac ultrasound used a 16-segment model to calculate the wall motion score, using a scale of 1 (normokinesis) to 4 (dyskinesis).[19] Apical wall motion score was calculated by averaging the four apical segments (septal, inferior, lateral, and anterior). These experts also carefully scrutinized images for the existence of apical mural thrombosis. We measured longitudinal myocardial strain from apical long-axis sequences using a six-segment model (EchoPAC) and obtained apical peak strain by averaging the instantaneous peak values from the mid anteroseptal, apical-septal, and apical-inferior segments. We measured the E-wave propagation index as the ratio between the E-wave velocity-time integral and LV length.[20] Other conventional echocardiographic data were obtained and measured following standardized recommendations.[19]

Stasis Mapping

We obtained the unsteady 2D blood flow field in the left ventricle using color Doppler velocimetry (CDV),[21] sometimes referred to as vector flow mapping.[22] Briefly, we acquired color Doppler sequences (eight to 14 beats) from the three-chamber view followed by B-mode sequences (four to six beats) at a high frame rate without tilting or displacing the probe. Under a planar flow assumption, CDV provides the crossbeam velocity component by integrating the continuity equation, using the tracked myocardial wall to set nonpenetration boundary conditions.

We assessed intraventricular blood stasis by generating spatiotemporal maps of the residence time (RT) of blood inside the left ventricle (Figure 1). The RT is a physical magnitude that accounts for the time that a volume of blood spends inside the chamber.[11] As previously shown, blood RT maps can be efficiently obtained in the left ventricle from unsteady 2D CDV data using an advection equation of a passive scalar with unit forcing.[5,11,23] We integrated this equation over eight consecutive cardiac cycles to ensure temporal convergence. From the RT maps, we calculated the average RT of the entire blood volume inside the left ventricle at the time of mitral valve opening of the last beat. This is a representative metric of global stasis that accounts for the full blood pool in the ventricle. However, local stasis metrics may be also meaningful for thrombosis. Therefore, we defined stagnant regions as those with RT $\geq$ 2 cardiac cycles and severely stagnant regions as those with RT $\geq$ 6 cardiac cycles (Figure 1).[23] Blood regions with RT $>$ 2 cycles are equivalent to the residual volume previously described in the literature[9] and have been recently linked to increased risk for LV mural thrombosis after AMI.[5] We measured the following features of stagnant and severely stagnant regions: (1) size relative to total LV size (area in two dimensions, as a percentage) and (2) its contact length with the endocardium (expressed a percentage of total endocardial length). The contact perimeter of stagnant regions accounts for flow-endocardium interactions that most intensively activate the coagulation cascade.[24] These features of stagnant regions were automatically measured at the instant of filling onset, and regions not spanning a full cardiac cycle or <2% of LV area were dismissed. Whenever more than one stagnant region was identified, only the one closest to the apex was analyzed. The reproducibility of these stasis metrics has been reported elsewhere.[23] We analyzed all echocardiographic and carotid Doppler data blinded to the other technique. An example of the CDV, RT maps, and ongoing HITS is shown in Figure 2.

Statistical Analysis

We analyzed differences among phases using linear mixed-effects models accounting for repeated measures. Least square means and their 95% CIs are reported for these models. We used Tukey's contrasts for comparison among phases. We assessed the association between the number of HITS and stasis indices using bivariate plots followed by linear or exponential regression analyses pooling AMI phase data. The 95% prediction intervals were calculated for these models. To assess the three-way interactions among AMI phase, stasis metrics, and the number of HITS, we used bivariate regression and mediation analyses.[25] We used logistic regression followed by receiver operating characteristic curve analysis to assess the capacity of RT to predict the incidence (one or more) of HITS. We selected the cutoff criterion on the basis of Youden's J statistic. Goodness-of-fit metrics of regression, mediation, and receiver operating characteristic analyses were corrected for overfitting using a bootstrap of 1,000 replicates. Statistical analysis was performed using R version 3.3.1 (R Foundation for Statistical Computing, Vienna, Austria). P values $<$ .05 were considered to indicate statistical significance.

RESULTS

Sequential AMIs induced progressive LV chamber dilatation and a decrease in LV ejection fraction (Table 1) from 61% (56%–66%) at baseline to 53% (48%–58%) and 47% (42%–52%) during AMI-1 and AMI-2 phases, respectively. Global and apical wall motion scores as well as apical peak longitudinal strain significantly worsened during AMI phases. Mural thrombosis was not detected in any animal. No HITS were detected at baseline. Instead, HITS were detected in five animals (50%) during AMI-1 phase and in nine animals (90%) during AMI-2 phase. The number of HITS detected during the 30 min of AMI-1 phase was 4 (0–9), subsequently increasing to 12 (7–18) during the 30 min of AMI-2 phase (Figure 3).

Concomitant with the number of HITS (Figures 2 and 3), global stasis increased with sequential AMIs; averaged RT was >30% higher during AMI-1 than at baseline (3.3 [2.9–3.7] cycles vs 2.4 [2.0–2.8] cycles, $P <$ .001), increasing even further during AMI-2 phase to 4.0 (3.6–4.4) cycles ($P <$ .001 vs baseline and AMI-1 phase). Small stagnant (RT $>$ 2 cycles) and severely stagnant (RT $>$ 6 cycles) regions were identified at baseline in 10 (100%) and four (40%) animals, respectively. Size and endocardial contact of these regions increased significantly during AMI. Of note, severely stagnant regions were more than twice as large by AMI-2 phase than at baseline, and their contact perimeter was on average 49% (41%–58%) of the total LV endocardial length (Table 1).

Apical wall motion score was the only conventional echocardiographic variable correlating with the number of HITS, but the correlation was weak (pooled AMI-1 and AMI-2 data; Table 2). On the

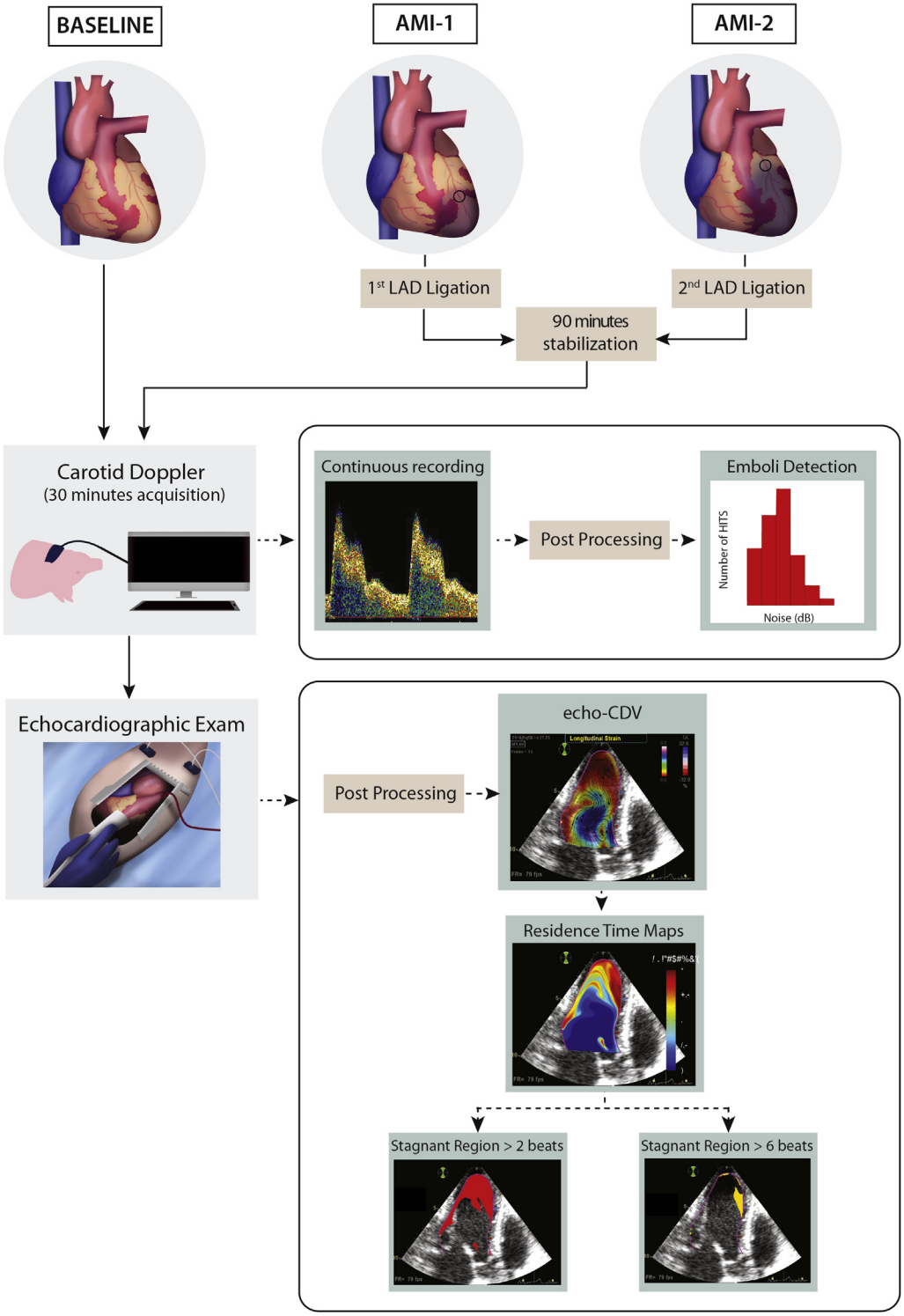

Figure 1 Experimental procedure and methodology.

contrary, most stasis metrics predicted the number of HITS during AMI (Table 2, Figure 4). The average RT was closely related to the number of HITS following an exponential fitting (bootstrap-adjusted $R = 0.87$, adjusted $R^2 = 0.77$, $y = -3.44 + 0.22 \times e^x$, $P < .001$; Figure 4). The bootstrap-adjusted area under the receiver operating characteristic curve of the average RT to identify microemboli (one or more HITS) was 0.89 (95% CI, 0.75–1.00). The cutoff of RT = 3.3 cycles showed 83% sensitivity (95% CI, 50%–100%) and 85% specificity (95% CI, 64%–100%) for predicting the appearance of HITS (Figure 5). By bivariate regression, the average RT ($P < .01$) and not the AMI phase category ($P = .60$) was significantly related to the number of HITS. Mediation analysis showed that the average RT accounted for 74% (95% CI, 33%–170%) of the effect of the AMI phase on the number of HITS ($P < .001$).

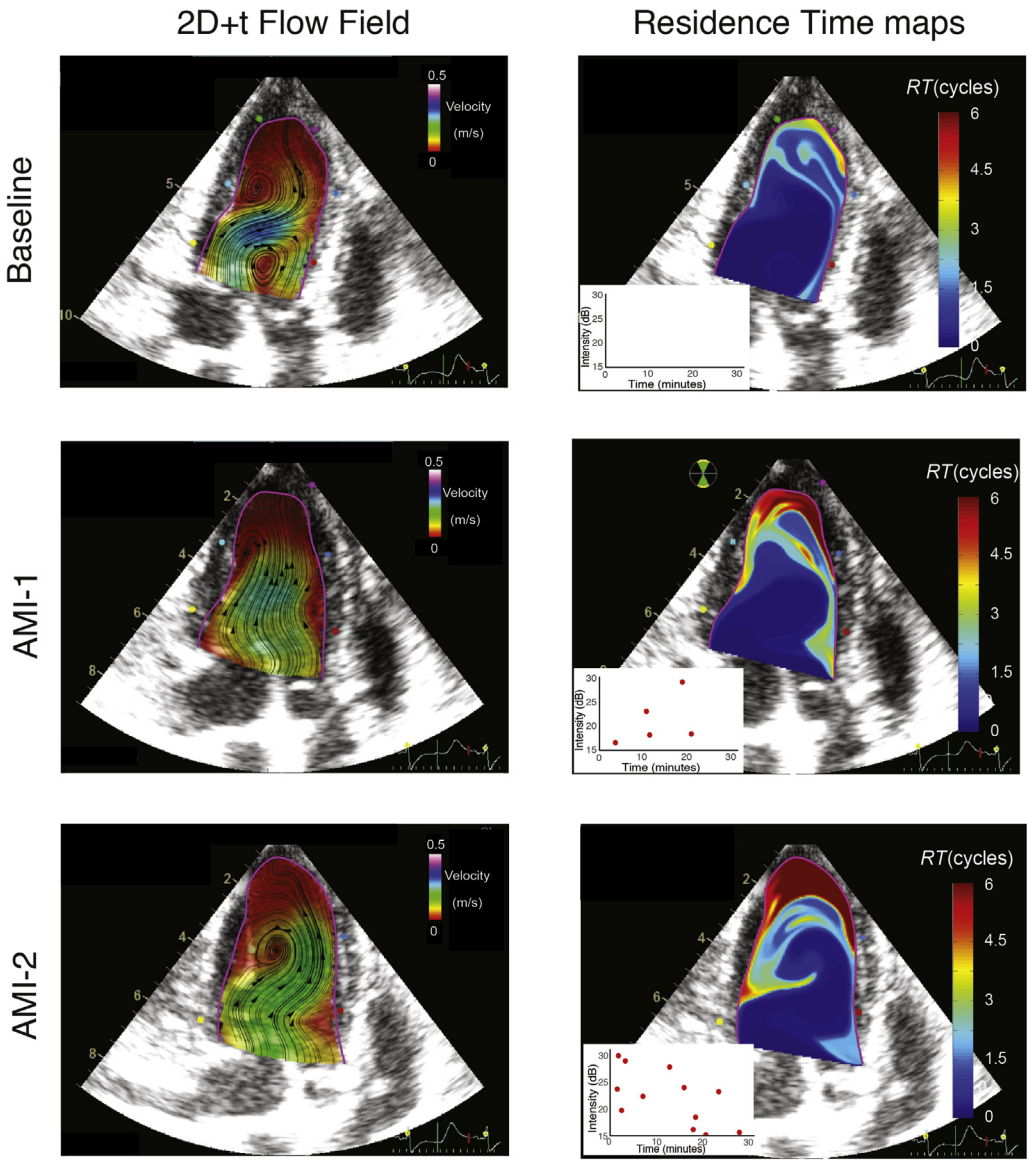

Figure 2 Representative intracardiac flow and stasis mapping example. Intraventricular time-dependent 2D flow (2D+t, first column) and blood RT maps in the left ventricle (second column) of a representative example, pig 4, during baseline (first row), AMI-1 (first AMI sequence, second row), and AMI-2 (second AMI sequence, third row) phases. For 2D+t flow mapping, the distributions of the flow velocity and instantaneous streamlines are overlaid on the total magnitude of flow velocity, from 0 m/sec (*black*) to 0.5 m/sec (*white*) and the raw B-mode tissue images. For the blood RT mapping images, the color scale represents the number of beats that each blood volume element remains inside the left ventricle, from zero cardiac cycles (*dark blue*) to six cardiac cycles (*dark red*). In both representations, a *cyan line* depicts the LV endocardium. Insets in RT maps: emboli detection (in decibels) during the 30-min acquisition.

DISCUSSION

To our knowledge, this is the first study demonstrating that cerebral microembolism due to cardiac disease can be predicted by an image-based assessment of intracardiac stasis. On the basis of the well-known relationship between stasis and the risk for intraventricular thrombosis, we exploited a bedside echocardiography-based technique to assess the risk for cardiac embolism. A good correlation was observed between the degree of blood stasis in the ventricle and the incidence of cerebral microembolisms, although intraventricular thrombus was not detectable using high-resolution epicardial ultrasound. These findings suggest a good potential of stasis imaging for predicting the risk for cardioembolic stroke in the absence of atrial fibrillation.

Intraventricular Stasis as a Source of Cardioembolism

Until recently, characterizing intracardiac stasis has been based almost exclusively on the visual interpretation of spontaneous contrast using B-mode ultrasound.[26] Unfortunately, this qualitative approach is highly subjective and equipment dependent. The development of flow-imaging modalities based on cardiac ultrasound, phase-contrast magnetic resonance, or computational fluid dynamics[27] allows deriving quantitative personalized metrics of global and regional intraventricular stasis.

Table 1 Conventional and stasis data derived from echocardiography

Variable	Baseline	AMI-1	AMI-2	ANOVA *P*
Heart rate, beats/min	64 (58 to 69)	59 (50 to 61)	53 (48 to 58)*	.01
Echocardiographic indices				
LV end-systolic volume, mL	17 (13 to 20)	24 (21 to 27)*	29 (25 to 32)*	<.001
LV end-diastolic volume, mL	42 (38 to 48)	51 (46 to 56)	55 (50 to 60)*	.005
LV ejection fraction, %	61 (56 to 66)	53 (48 to 58)*	47 (42 to 52)*	<.001
Stroke volume, mL	26 (22 to 30)	27 (23 to 30)	26 (22 to 30)	.80
E-wave velocity, m/sec	0.73 (0.63 to 0.83)	0.72 (0.61 to 0.82)	0.57 (0.46 to 0.68)	.04
A-wave velocity, m/sec	0.68 (0.58 to 0.79)	0.62 (0.52 to 0.72)	0.55 (0.43 to 0.66)	.10
E-wave propagation index	2.0 (1.7 to 2.2)	2.0 (1.8 to 2.3)	1.8 (1.6 to 2.1)	.60
Wall motion score				
Global wall motion score	17.0 (15.7 to 18.3)	27.3 (26.0 to 28.6)*	34.4 (33.1 to 35.7)*,†	<.001
Apical wall motion score	5.0 (4.3 to 5.7)	14.4 (13.6 to 15.2)*	17.2 (16.4 to 17.9)*,†	<.001
Strain				
Global peak longitudinal strain, %	−16.6 (−18.5 to −14.8)	−14.7 (−16.4 to −12.9)	−13.5 (−15.3 to −11.8)*	.01
Apical peak longitudinal strain, %	−16.7 (−21.1 to −12.3)	−11.8 (−15.7 to −7.9)	−8.2 (−12.4 to −4.1)*	.02
Stasis				
Average RT, cycles	2.4 (2.0 to 2.8)	3.3 (2.9 to 3.7)*	4.0 (3.6 to 4.4)*,†	<.001
Size of stagnant regions, %	46 (40 to 53)	54 (47 to 60)*	62 (55 to 68)*,†	<.001
Endocardial contact of stagnant regions, %	56 (47 to 66)	64 (54 to 74)	69 (59 to 78)	.10
Size of severely stagnant regions, %	12 (5 to 20)	24 (16 to 31)*	34 (27 to 41)*,†	<.001
Endocardial contact of severely stagnant regions, %	20 (11 to 29)	33 (24 to 41)	49 (41 to 58)*,†	<.001

Data are expressed as least square mean estimate (95% CI).
*$P < .05$ vs baseline.
†$P < .05$ between AMI-1 and AMI-2.

Avoidance of blood retention is believed to be one of the teleological advantages of the complex flow patterns observed in the human heart.[28] The vortex ring that develops during diastole has a prominent role in transporting blood and is a major contributor to filling.[29] However, in the setting of an AMI, impaired wall motion and/or LV remodeling may disturb the physiologic flow trajectories that facilitate blood washout.[9,10] If the ventricle dilates, although the vortex grows, its propagation along the long axis of the left ventricle becomes impaired. The net effect is that the fresh blood carried by the vortex reduces its interaction with apical blood.[30] Remarkably, the risk for mural thrombosis after AMI has been associated with the degree of apical propagation of the passive filling column,[20] as well as the location and pulsatility of the diastolic vortex.[31] However, additional factors beyond wall motion[6] and early apical flow propagation[20] have been reported to influence blood washout.[23]

Importantly, stagnant regions may activate the coagulation cascade without macroscopic wall thrombosis ever being detected, either because a small mural thrombus is missed or because the thrombotic material embolizes before the patient is scanned. In fact, a large proportion of ischemic strokes after AMI take place after the patient is discharged,[2] and protocols of serial imaging to rule out mural thrombosis are difficult to implement. Furthermore, contrast-enhanced magnetic resonance identifies LV mural thrombosis in fewer than one third of patients with histories of AMI who experience ischemic strokes of undetermined source.[32] These observations call for improvement in a personalized assessment of cardioembolic stroke in the absence of atrial fibrillation. Interestingly, stasis metrics such as those presented here could be combined with local and systemic variables of coagulation activation to obtain integrated, patient-specific biomechanical markers of overall thrombotic risk.[24,31]

Cerebral Microembolism during AMI

An abnormal incidence of HITS has been reported in the setting of stroke, valvular and coronary heart diseases, atrial fibrillation, and mechanical valves.[13,33] One of the few works studying microembolism during AMI reported an incidence of HITS in as many as 17% of patients, finding an association of these results with reduced ejection fraction and wall motion alterations. However, remarkably, 80% of patients had cerebral microemboli without evidence of mural thrombosis.[14] Unfortunately, data unequivocally relating all cases of cardioembolic stroke to mural thrombosis are lacking. Evidence from the field of paroxysmal atrial fibrillation further calls for examining the classical paradigm that cardioembolic stroke results from the dislodgement of a mural thrombus induced by abnormal wall motion.[34]

The clinical significance of HITS is still a matter of debate, although there is strong evidence relating cerebral microemboli to

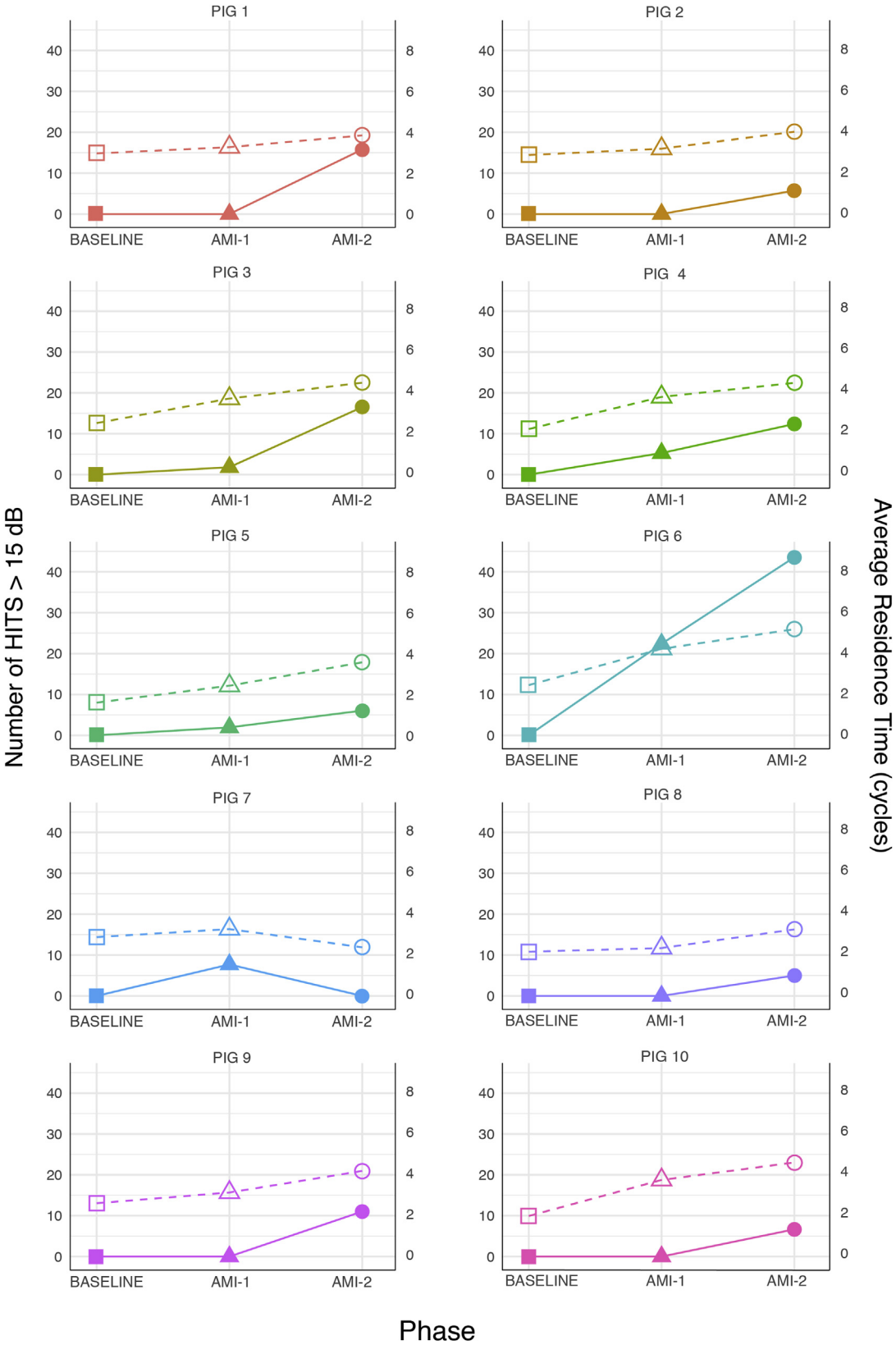

Figure 3 HITS and average RT in the left ventricle during the experimental phases for each animal. The number of HITS is plotted in *filled symbols* and *solid lines* against the left vertical axes, whereas the RT is plotted in *open symbols* and *dashed lines* against the right vertical axes.

Table 2 Univariate linear regression analyses between the number of HITS and the conventional echocardiographic and stasis indices

Variable	*R*	*P*
Conventional indices		
Heart rate	0	.80
LV end-systolic volume	0	.20
LV end-diastolic volume	0	.10
LV ejection fraction	0.22	.80
Wall motion score		
Global wall motion score	0.20	.05
Apical wall motion score	0.30	.04
Strain		
Global peak longitudinal strain	0	.70
Apical peak longitudinal strain	0	.20
Stasis		
Average RT in the left ventricle, linear	0.67	<.001
Average RT in the left ventricle, exponential	0.87	<.001
Size of the stagnant regions	0.30	.04
Endocardial contact of stagnant regions	0.29	.05
Size of the severely stagnant regions	0.73	<.001
Endocardial contact of severely stagnant regions	0.33	.02

Data are shown for pooled AMI-1 and AMI-2 phases.

silent brain infarcts,[35] and the latter is a well-established predictor of ischemic stroke, dementia, and cognitive dysfunction.[15] Moreover, HITS have been associated with the decline of neurologic function after coronary artery bypass surgery as well as with early recurrence of stroke.[36] On this basis, HITS are frequently used as surrogate end points for early clinical trials aimed to reduce cardioembolic stroke.[16] In animal experimental studies, such as ours, detection of HITS has been useful to demonstrate the role of mechanical prosthetic valve orientation.[13] We believe this previous evidence justifies choosing HITS as a surrogate marker of embolism.

Clinical Implications

The need for intense antiplatelet therapy after intracoronary stenting substantively increases hemorrhagic risk if anticoagulation therapy is also required. Consequently, anticoagulation after AMI is indicated only when atrial fibrillation or LV thrombus is identified.[37] Although not tested in the present study, anticoagulation therapy reduces the cardioembolic risk, and stasis mapping could be useful for early stratification of patients. The present study confirms preliminary clinical evidence showing that flow imaging is superior to conventional metrics such as ejection fraction and regional wall motion in predicting intraventricular thrombotic complications during acute anterior AMI.[5] In the present study we focused on echocardiographic assessment of flow alterations in the left ventricle after AMI. However, stasis mapping can be applicable to other heart chambers and cardiac conditions and can be achieved by other imaging modalities such as phase-contrast magnetic resonance[11] and computational fluid dynamics.[24] A currently ongoing prospective clinical trial (ClinicalTrials.gov identifier NCT02917213) will eventually establish the potential clinical efficacy of these techniques.

Limitations

LV flow is three-dimensional, but in the present study we used a 2D approach. Although a planar flow simplification may lead to inaccuracy, 2D methods have practical advantages. First, computational requirements are markedly reduced when implemented in two dimensions.[11] Second, bedside echocardiography is a much more accessible in the setting of AMI than phase-contrast magnetic resonance. We have shown that the key spatial features and numeric values of RT are well represented in the long-axis three-chamber plane imaged on 2D CDV.[11] Thus, we do not believe that the main conclusions of our study would change qualitatively when using three-dimensional techniques.

Stasis mapping and its derived metrics are highly dependent on image quality. Therefore, when using transthoracic echocardiography in the setting of AMI, stasis metrics must be interpreted with caution if optimal apical visualization is unavailable. Nevertheless, preliminary data from our group suggest that this is not a major limitation in the clinical setting.[5] In the present work we used a LAD ligation AMI model, which may induce different mechanical responses than the ones found in patients with AMI in clinical practice. Also, we evaluated stasis mapping and HITS incidence in a porcine model, and therefore, our results may not be directly transferable to human patients.

Because several stasis metrics were tested, we cannot exclude a certain degree of overfitting in our results. The detection of HITS was performed using a bigate probe at a fixed frequency of 8 MHz, a method that is unable to differentiate between gaseous and solid embolus. However, our study was designed and conducted to avoid potential catheterization-related confounders. Antithrombotic therapy, as routinely used in the clinical setting of AMI, may eventually lower the incidence of HITS, without affecting stasis metrics. We intentionally avoided antithrombotic treatment in our experiments so as not to jeopardize the power of our study. Consequently, the absolute cutoff values of stasis metrics to predict HITS may be different in the presence of antithrombotic treatment.

CONCLUSION

Stasis imaging is a useful technique to detect increased intraventricular blood retention in the heart. During an anterior AMI, severe blood transport abnormalities and stasis take place inside the left ventricle. These factors prolong the RT of blood in the left ventricle, which correlates with the rate of microemboli detected by transcarotid Doppler. If these findings are confirmed in the clinical setting and in the presence of antithrombotic treatment, stasis mapping may become a useful tool to assess the risk for embolism in the setting of AMI and potentially in other heart disease conditions.

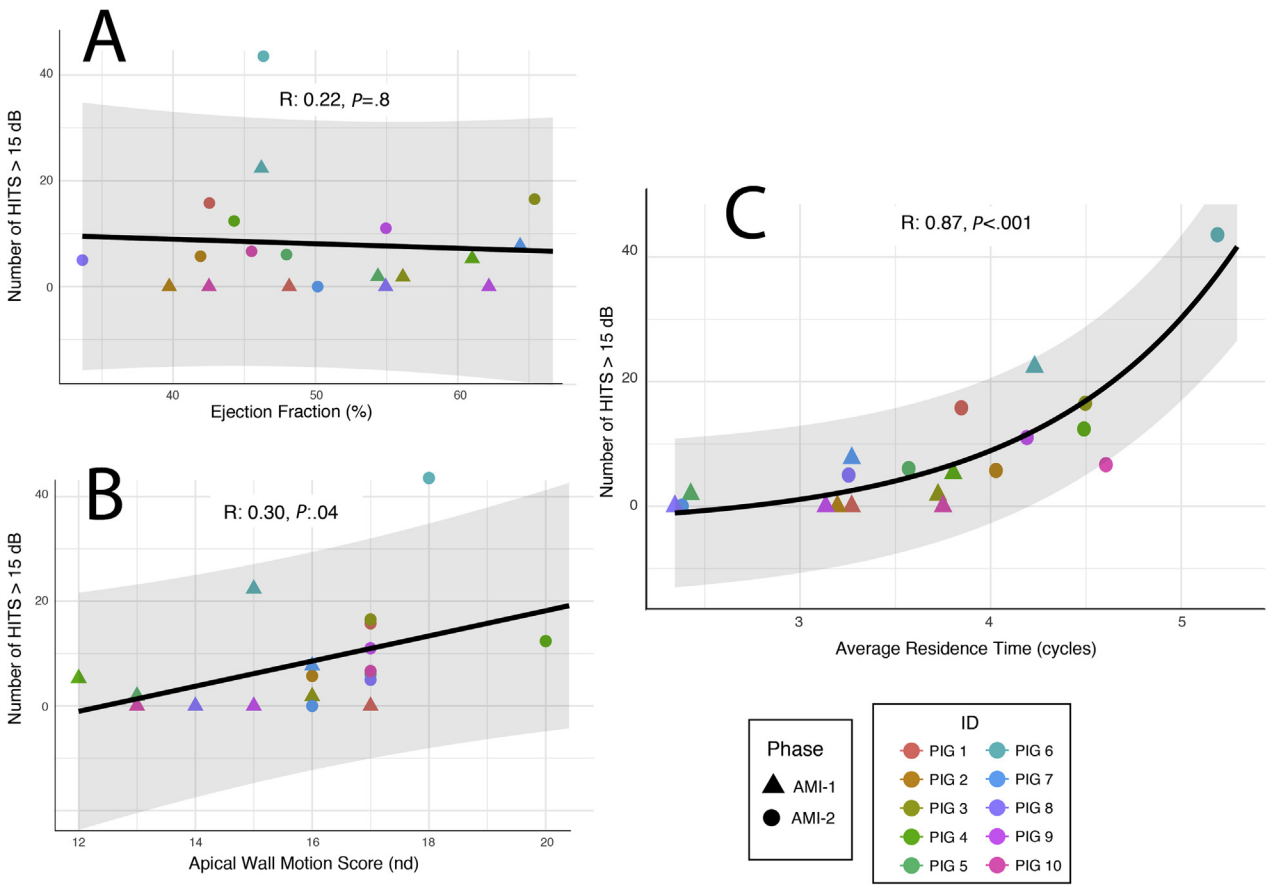

Figure 4 Relationships between HITS and echocardiographic indices. **(A)** Relationship between HITS and LV ejection fraction. **(B)** Relationship between HITS and apical wall-motion score. **(C)** Relationship between HITS and the average RT. The *solid black lines* indicate the fittings, and the *shadowed areas* indicate their 95% CI for prediction.

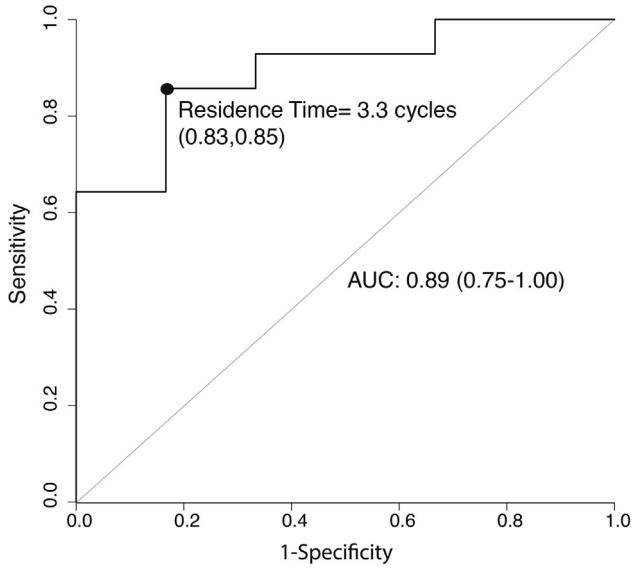

Figure 5 Diagnostic performance of stasis indices. Receiver operating characteristic (ROC) curves for the average RT in the left ventricle for the diagnosis of HITS. *AUC*, Area under the curve.

ACKNOWLEDGMENTS

We are indebted to all the personnel of the Department of Experimental Medicine and Surgery of the Hospital General Universitario Gregorio Marañón for their support in the animal experiments and to Diana Bóveda for her assistance and artwork in Figure 1.

REFERENCES

1. Witt BJ, Ballman KV, Brown RD Jr., Meverden RA, Jacobsen SJ, Roger VL. The incidence of stroke after myocardial infarction: a meta-analysis. Am J Med 2006;119:354.e1-9.
2. Ferreira JP, Girerd N, Gregson J, Latar I, Sharma A, Pfeffer MA, et al. Stroke risk in patients with reduced ejection fraction after myocardial infarction without atrial fibrillation. J Am Coll Cardiol 2018;71:727-35.
3. Adams PC, Cohen M, Chesebro JH, Fuster V. Thrombosis and embolism from cardiac chambers and infected valves. J Am Coll Cardiol 1986;8:76B-87B.
4. Gellen B, Biere L, Logeart D, Lairez O, Vicaut E, Furber A, et al. Timing of cardiac magnetic resonance imaging impacts on the detection rate of left ventricular thrombus after myocardial infarction. JACC Cardiovasc Imaging 2017;10:1404-5.

5. Martinez-Legazpi P, Rossini L, Perez Del Villar C, Benito Y, Devesa-Cordero C, Yotti R, et al. Stasis mapping using ultrasound: a prospective study in acute myocardial infarction. JACC Cardiovasc Imaging 2018; 11:514-5.
6. Weinsaft JW, Kim J, Medicherla CB, Ma CL, Codella NC, Kukar N, et al. Echocardiographic algorithm for post-myocardial infarction LV thrombus: a gatekeeper for thrombus evaluation by delayed enhancement CMR. JACC Cardiovasc Imaging 2016;9:505-15.
7. Melamed KH, Goldhaber SZ. Inflammation and myocardial infarction. Circulation 2014;130:e334-6.
8. Shen WF, Tribouilloy C, Rida Z, Peltier M, Choquet D, Rey JL, et al. Clinical significance of intracavitary spontaneous echo contrast in patients with dilated cardiomyopathy. Cardiology 1996;87:141-6.
9. Bolger AF, Heiberg E, Karlsson M, Wigstrom L, Engvall J, Sigfridsson A, et al. Transit of blood flow through the human left ventricle mapped by cardiovascular magnetic resonance. J Cardiovasc Magn Reson 2007;9: 741-7.
10. Hendabadi S, Bermejo J, Benito Y, Yotti R, Fernandez-Aviles F, Del Alamo JC, et al. Topology of blood transport in the human left ventricle by novel processing of Doppler echocardiography. Ann Biomed Eng 2013;41:2603-16.
11. Rossini L, Martinez-Legazpi P, Vu V, Fernandez-Friera L, Perez Del Villar C, Rodriguez-Lopez S, et al. A clinical method for mapping and quantifying blood stasis in the left ventricle. J Biomech 2016;49:2152-61.
12. Stygall J, Kong R, Walker JM, Hardman SM, Harrison MJ, Newman SP. Cerebral microembolism detected by transcranial Doppler during cardiac procedures. Stroke 2000;31:2508-10.
13. Kleine P, Perthel M, Hasenkam JM, Nygaard H, Hansen SB, Laas J. Downstream turbulence and high intensity transient signals (HITS) following aortic valve replacement with Medtronic Hall or St. Jude Medical valve substitutes. Eur J Cardiothorac Surg 2000;17:20-4.
14. Nadareishvili ZG, Choudary Z, Joyner C, Brodie D, Norris JW. Cerebral microembolism in acute myocardial infarction. Stroke 1999;30:2679-82.
15. Vermeer SE, Prins ND, den Heijer T, Hofman A, Koudstaal PJ, Breteler MM. Silent brain infarcts and the risk of dementia and cognitive decline. N Engl J Med 2003;348:1215-22.
16. von Bary C, Deneke T, Arentz T, Schade A, Lehrmann H, Fredersdorf S, et al. Online measurement of microembolic signal burden by transcranial Doppler during catheter ablation for atrial fibrillation: results of a multicenter trial. Front Neurol 2017;8:131.
17. Klement P, Berry LR, Liao P, Wood H, Tressel P, Smith LJ, et al. Antithrombin-heparin covalent complex reduces microemboli during cardiopulmonary bypass in a pig model. Blood 2010;116:5716-23.
18. Ringelstein EB, Droste DW, Babikian VL, Evans DH, Grosset DG, Kaps M, et al. Consensus on microembolus detection by TCD. International Consensus Group on Microembolus Detection. Stroke 1998;29:725-9.
19. Lang RM, Badano LP, Mor-Avi V, Afilalo J, Armstrong A, Ernande L, et al. Recommendations for cardiac chamber quantification by echocardiography in adults: an update from the American Society of Echocardiography and the European Association of Cardiovascular Imaging. J Am Soc Echocardiogr 2015;28:1-39.e14.
20. Harfi TT, Seo JH, Yasir HS, Welsh N, Mayer SA, Abraham TP, et al. The E-wave propagation index (EPI): a novel echocardiographic parameter for prediction of left ventricular thrombus. Derivation from computational fluid dynamic modeling and validation on human subjects. Int J Cardiol 2017;227:662-7.
21. Garcia D, Del Alamo JC, Tanne D, Yotti R, Cortina C, Bertrand E, et al. Two-dimensional intraventricular flow mapping by digital processing conventional color-Doppler echocardiography images. IEEE Trans Med Imaging 2010;29:1701-13.
22. Uejima T, Koike A, Sawada H, Aizawa T, Ohtsuki S, Tanaka M, et al. A new echocardiographic method for identifying vortex flow in the left ventricle: numerical validation. Ultrasound Med Biol 2010;36:772-88.
23. Benito Y, Martinez-Legazpi P, Rossini L, Pérez del Villar C, Yotti R, Martín Peinador Y, et al. Age-dependence of flow homeostasis in the left ventricle. Front Physiol 2019;10:485.
24. Seo JH, Abd T, George RT, Mittal R. A coupled chemo-fluidic computational model for thrombogenesis in infarcted left ventricles. Am J Physiol Heart Circ Physiol 2016;310:H1567-82.
25. VanderWeele TJ, Vansteelandt S. Mediation analysis with multiple mediators. Epidemiol Meth 2014;2:95-115.
26. Weinsaft JW, Kim RJ, Ross M, Krauser D, Manoushagian S, LaBounty TM, et al. Contrast-enhanced anatomic imaging as compared to contrast-enhanced tissue characterization for detection of left ventricular thrombus. JACC Cardiovasc Imaging 2009;2:969-79.
27. Bermejo J, Martinez-Legazpi P, Alamo JCd. The clinical assessment of intracardiac flows. Ann Rev Fluid Mech 2015;47.
28. Kilner PJ, Yang GZ, Wilkes AJ, Mohiaddin RH, Firmin DN, Yacoub MH. Asymmetric redirection of flow through the heart. Nature 2000;404: 759-61.
29. Martinez-Legazpi P, Bermejo J, Benito Y, Yotti R, Perez Del Villar C, Gonzalez-Mansilla A, et al. Contribution of the diastolic vortex ring to left ventricular filling. J Am Coll Cardiol 2014;64:1711-21.
30. Bermejo J, Benito Y, Alhama M, Yotti R, Martinez-Legazpi P, Pérez del Villar C, et al. Intraventricular vortex properties in non-ischemic dilated cardiomyopathy. Am J Physiol Heart Circ Physiol 2014;306:H718-29.
31. Son JW, Park WJ, Choi JH, Houle H, Vannan MA, Hong GR, et al. Abnormal left ventricular vortex flow patterns in association with left ventricular apical thrombus formation in patients with anterior myocardial infarction: a quantitative analysis by contrast echocardiography. Circ J 2012;76:2640-6.
32. Takasugi J, Yamagami H, Noguchi T, Morita Y, Tanaka T, Okuno Y, et al. Detection of Left ventricular thrombus by cardiac magnetic resonance in embolic stroke of undetermined source. Stroke 2017;48:2434-40.
33. Sliwka U, Job FP, Wissuwa D, Diehl RR, Flachskampf FA, Hanrath P, et al. Occurrence of transcranial Doppler high-intensity transient signals in patients with potential cardiac sources of embolism. A prospective study. Stroke 1995;26:2067-70.
34. Brambatti M, Connolly SJ, Gold MR, Morillo CA, Capucci A, Muto C, et al. Temporal relationship between subclinical atrial fibrillation and embolic events. Circulation 2014;129:2094-9.
35. Goldberg I, Auriel E, Russell D, Korczyn AD. Microembolism, silent brain infarcts and dementia. J Neurol Sci 2012;322:250-3.
36. Valton L, Larrue V, le Traon AP, Massabuau P, Geraud G. Microembolic signals and risk of early recurrence in patients with stroke or transient ischemic attack. Stroke 1998;29:2125-8.
37. Ibanez B, James S, Agewall S, Antunes MJ, Bucciarelli-Ducci C, Bueno H, et al. 2017 ESC guidelines for the management of acute myocardial infarction in patients presenting with ST-segment elevation: the Task Force for the Management of Acute Myocardial Infarction in Patients Presenting with ST-Segment Elevation of the European Society of Cardiology (ESC). Eur Heart J 2018;39:119-77.